# Compact UWB MIMO Antenna With High Isolation Using Fence-Type Decoupling Structure

Lili Wang, Zhonghong Du, Hailong Yang, Ruoyan Ma, Yuchen Zhao, Xueqi Cui, and Xiaoli Xi, *Member, IEEE*

***Abstract*—In this letter, an ultrawideband (UWB) multiple-input–multiple-output (MIMO) antenna using a novel fence-type decoupling structure, which has high isolation in the UWB, is presented. The MIMO design consists of two half-cutting UWB antenna units that have good low-frequency impedance-matching performance because of the use of a rectangular slot on the radiation patch. Meanwhile, the isolation in the operating band is enhanced by introducing the fence-type decoupling structure at the ground of the antenna. Furthermore, the L-shaped parasitic branches are designed to heighten the impedance bandwidth and isolation in the low-frequency band, i.e., 3–3.4 GHz. The simulation and experiments show that the antenna has low mutual coupling ($S_{21} <$ –25 dB) and a low envelope correlation coefficient (ECC $<$ 0.004) in the UWB.**

***Index Terms*—Fence-type decoupling structure, high isolation, multiple-input–multiple-output (MIMO), ultrawideband (UWB) antenna.**

## I. Introduction

ULTRAWIDEBAND (UWB) technology has been widely studied due to its high transmission rate, strong anti-interference, and easy fabrication [1]. Nevertheless, the highest radiated power spectral density in the Federal Communications Commission approved 3.1–10.6 GHz band is stipulated to be below −41.3 dBm/MHz, which will result in more serious fading of signals in multipath environments and deterioration of the performance of the UWB system [2]. Multiple-input–multiple-output (MIMO) is a diversity technique using multiple transmitting antennas and receiving antennas. The technique can effectively decompose the communication link into several parallel subcommunication channels, turn the multipath fading, which is not conducive, to wireless communication into a favorable factor, and improve the reliability of the data transmission in the system [3], [4]. However, there will be a serious coupling problem when multiple antennas are installed in portable devices with small space, which will seriously affect the performance of diversity. Therefore, to guarantee the excellent function of the antenna in an MIMO communication system, the MIMO antenna must have higher isolation. Moreover, designing a high-isolation MIMO antenna in portable devices is a challenging task [5].

In recent years, many technologies [6]–[15] have been proposed to heighten the isolation of MIMO antennas, such as the neutralization line [6], [7], electromagnetic band-gap structure [8], diversity technique [9], [10], insertion of a decoupling structure on the ground [11], [12], defected ground structure [13], [14], and partial ground plane [15].

In [9], a UWB antenna with a size of 28 × 50 mm$^2$ was proposed. The mutual coupling of the MIMO antenna is less than −18 dB when using spatial angle variation techniques, but the isolation of the antenna is still less than that in most of the literature [11], [13], [15]. In [14], an antenna with a size of 60 × 95 mm$^2$ was designed; it achieved more than 18 dB of isolation by etching the defected ground structure. However, the operating frequency of the antenna in [14] is 2.5–4.5 GHz, which is not satisfactory for UWB communication. In [11], the isolation of the operating band was enhanced by inserting an H-type decoupling structure. The isolation of the antenna has been improved ($S_{21} >$ 25 dB), but the size is still greater than that in most of the literature [7]–[14]. As in [15], although the antenna has achieved better isolation, the size is larger, which is not conducive to integration in smaller systems. The isolation and size of the MIMO antenna are $S_{21} >$ 22 dB and 38 × 91 mm$^2$, respectively.

A UWB MIMO antenna using a fence-type decoupling structure to achieve high isolation is proposed in this letter. The fence-type decoupling structure is mainly composed of many slits of equal size. The multiple slits are equivalent to a band-stop filter, which can effectively weaken the coupling current between the ports. The microstrip lines connected to these slits are divided into three segments, which are used to increase the path of the coupling current and decrease the mutual coupling of the antenna. Although the fence-type decoupling structure can significantly enhance the isolation of the MIMO antenna, the isolation and impedance matching of the antenna at 3.1 GHz are not ideal. Therefore, two L-shaped parasitic branches are introduced at the top of the dielectric plate to improve the phenomenon. Finally, to verify the reliability of the simulation results of the design, a prototype antenna is fabricated and tested. The measured results indicate that the MIMO antenna has higher isolation ($S_{21}$ $>$ 25 dB) and lower envelope correlation coefficient (ECC $<$ 0.004). In addition, the proposed antenna also has other outstanding features, such as a wider operating bandwidth (3–11 GHz, 114%), stable gain, and compact size of 50 × 35 mm$^2$.

Manuscript received June 2, 2019; revised June 20, 2019; accepted June 26, 2019. Date of publication July 1, 2019; date of current version August 2, 2019. This work was supported in part by the National Defense Pre-Research Foundation of China under Grant 6140450010302, in part by the National Natural Science Foundation of China under Grant 61701398, and in part by the Key Research and Development Plan of Shaanxi Province under Grant 2017ZDXM-GY-117. *(Corresponding author: Hailong Yang.)*

L. Wang, Z. Du, H. Yang, Y. Zhao, X. Cui, and X. Xi are with the Xi'an University of Technology, Xi'an 710048, China (e-mail: wanglili@xaut.edu.cn; duzhonghong00@163.com; yanghl68@163.com; zhaoyuchen@xaut.edu.cn; 892969971@qq.com; xixiaoli@xaut.edu.cn).

R. Ma is with the South China University of Technology, Guangzhou 510000, China (e-mail: 1536517478@qq.com).

Digital Object Identifier 10.1109/LAWP.2019.2925857

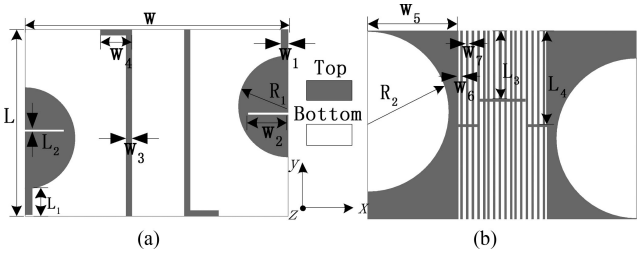


Fig. 1. Proposed design structure. (a) Top. (b) Bottom.

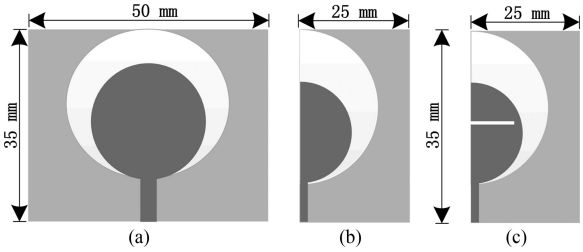


Fig. 2. Evolution of the single UWB antenna.

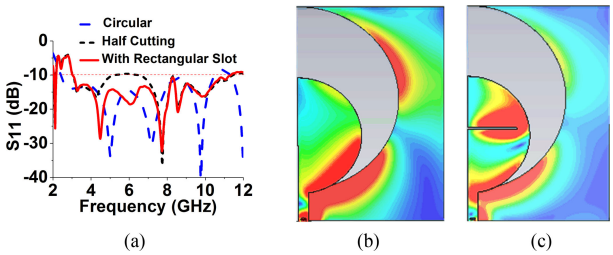


Fig. 3. (a) $S_{11}$ of a single antenna in different structures. Current distribution of the antenna (b) without and (c) with a rectangular slot at 6 GHz.

## II. Antenna Design and Analysis

The final UWB MIMO antenna geometry is displayed in Fig. 1. The proposed design was printed on an FR4 substrate of thickness $h = 1.0$ mm and relative permittivity $\varepsilon_r = 4.3$. The antenna consists of a half-cutting circular radiation patch at the top of the dielectric substrate, two L-shaped parasitic branches, and a fence-type decoupling structure at the bottom. The proposed antenna is designed in three steps. In this section, we discuss the evolution of the proposed design, including the element of the UWB antenna, the decoupling structure of the antenna, and the L-shaped parasitic branches.

### A. Single UWB Antenna

The evolution of the single UWB antenna is shown in Fig. 2. As far as we know, to ensure the omnidirectional and symmetry of the antenna pattern, most UWB antennas reported in [16] and [17] are designed to be symmetrical, which makes the antenna size larger. A small UWB antenna is needed in the UWB system, and many miniaturization methods have been reported in the literature [18], [19]. In this letter, the half-cutting technique is utilized to reduce the size of the antenna, as illustrated in Fig. 2(b), in which the dimensions of the half-cutting antenna are $35 \times 25$ mm$^2$. Compared with the antenna in Fig. 2(a), the size of the antenna in Fig. 2(b) is reduced by 50%. It is obvious from Fig. 3(a) that the *S*-parameters of the antenna in Fig. 2(b) are basically the same as those of the antenna in Fig. 2(a), but the impedance characteristic of the antenna is not ideal in the range of 5–7 GHz. Hence, to further improve the impedance-matching characteristics of the frequency band, a rectangular slot is embedded on the surface of the radiation patch, as depicted in Fig. 2(c). The rectangular slot [20] is etched on the radiation patch, which can provide an additional resonant mode to improve the impedance at 5–7 GHz. To better explain the effect of the rectangular slot on the resonant performance of the proposed design, Fig. 3(b) and (c) shows the current distribution of the antenna with or without rectangular slots on the radiating patch at 6 GHz. By comparing Fig. 3(b) with Fig. 3(c), we can find that the surface current is distributed along the edge of the rectangular slot when the rectangular slot is etched on the radiation patch. Therefore, the impedance matching of the MIMO antenna at 5–7 GHz is enhanced due to the resonance characteristics of the rectangular slot structure.

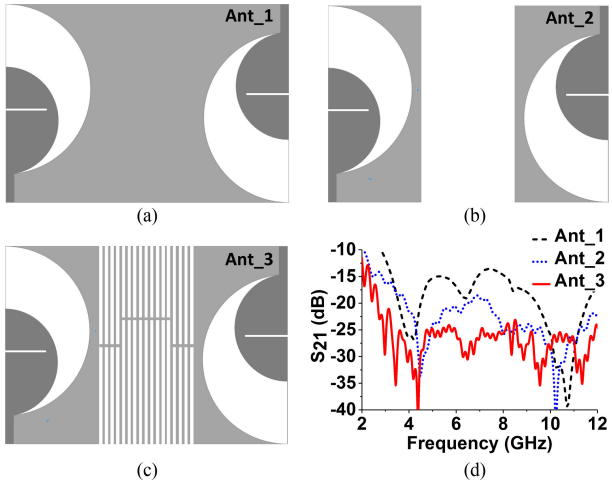


Fig. 4. (a)–(c) Configurations of ant_1, ant_2, and ant_3, respectively. (d) $S_{21}$ of ant_1, ant_2, and ant_3.

### B. Decoupling Structure Design

To overcome the multipath effect of the UWB system, two half-cutting UWB antennas are inverted to obtain the original UWB MIMO ant_1, as shown in Fig. 4(a). Fig. 4(d) shows that the coupling of the MIMO ant_1 without any decoupling structure is approximately $-15$ dB, which is still not ideal. Fig. 4(b) (ant_2) uses a rectangular defect ground structure. The isolation of ant_2 is greater than 25 dB at 5–8 GHz, which does not meet the requirements of this letter for high isolation. Hence, in Fig. 4(c) (ant_3), a fence-type decoupling structure composed of 16 slits, which extends the current path of the antenna so that the isolation of the MIMO antenna is more than 25 dB in the UWB, is designed. Fig. 4(d) clearly shows that the isolation of ant_3 is improved compared to that of ant_1 and ant_2. From a circuit perspective, the slits can be equivalent to a band-stop filter, which shows high-impedance characteristics in the UWB. It can be concluded that the fence-type structure plays a key role in restraining the mutual coupling of surface waves on the ground [14].

The fence-type structure plays an extremely key role in improving the isolation of the proposed antenna. Therefore, it is necessary to discuss the effect of the parameters of the fence-type slit structure on the antenna performance. In this letter, the influence of different numbers of slits on the isolation property

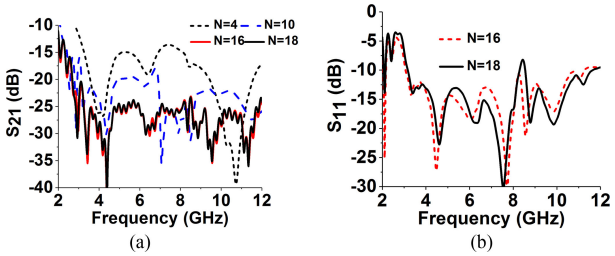


Fig. 5. (a) and (b) Influence of different numbers of slits on *S*-parameters.

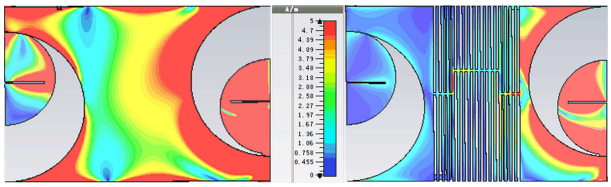


Fig. 6. Current distributions at 7.5 GHz. (a) ant_1. (b) ant_3.

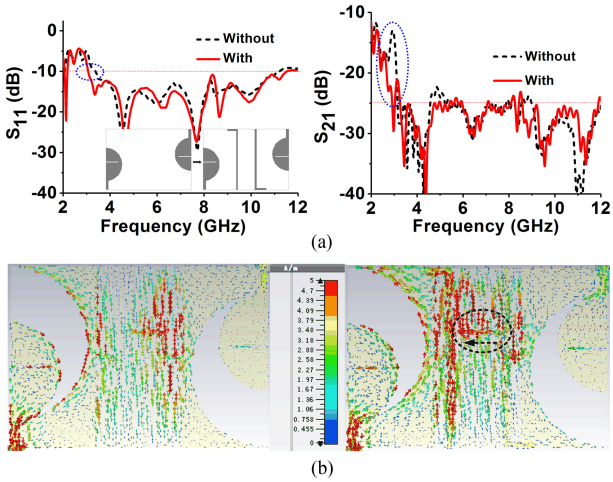


Fig. 7. (a) *S*-parameter and (b) current distributions at 3.2 GHz of the MIMO antenna with and without the L-shaped parasitic branch.

of the proposed antenna is compared. A fixed antenna geometry is assumed, and the antenna isolation is simulated when the numbers of slits are 4, 10, 16, and 18. As depicted in Fig. 5(a), the $S_{21}$ of the antenna gradually decreases over the entire operating bandwidth when the number of slits is increased, especially in the bandwidth of 4.3–7 GHz. When the number of slits is 16, the $S_{21}$ of the proposed antenna in the operating bandwidth is greater than 25 dB. As the number of slits increases, the electrical distance between the antenna elements gradually increases; thus, the mutual coupling of the MIMO antenna is reduced. Observing Fig. 5(b), when the number of slits is greater than 16, the impedance matching of a single UWB antenna is changed. Therefore, the number of ground slits selected is 16, which satisfies the design requirements of isolation and a compact size of the MIMO antenna.

To better understand the working mechanism of the antenna more intuitively, the current distribution of the two antennas at 7.5 GHz are given. The antenna unit on the right is connected to the excitation source, and the antenna unit on the left is connected to a load of 50 Ω. Observing Fig. 6, when ant_1 does not add any decoupling structure, there is much ground current flowing from the right antenna unit to the left antenna unit. Nevertheless, ant_3 restricts a large amount of the ground current from the right antenna unit to the left antenna unit via the slit structure; hence, the ground current to the left antenna unit is greatly reduced compared with that for ant_1 and ant_2. After comparison and analysis of the current distributions of the two kinds of antennas, the conclusion is in agreement with the simulation results of the $S_{21}$ parameters. It can be proven that the fence-type slot is an effective decoupling structure that can enhance the isolation of the proposed antenna.

### C. L-Shaped Parasitic Branches

Although the isolation of the proposed design is significantly heightened ($S_{21} > 25$ dB) after introducing the fence-type decoupling structure, the operating bandwidth is 3.4–11 GHz, which cannot be applied to UWB (3.1–10.6 GHz) systems. Observing the inset of Fig. 7(a), the L-shaped parasitic branches are designed to further heighten the impedance matching and isolation at 3.0–3.4 GHz. In Fig. 7(a), it can be seen that the L-shaped parasitic branches can change the resonant frequency of the proposed antenna (3.4–3.1 GHz). Meanwhile, the L-shaped parasitic branches also decrease the mutual coupling of the proposed design. In particular, the isolation is reduced by 69% (−13 to −22 dB) in the 3–3.4 GHz operating frequency band. The parasitic branches can form a resonant loop by electromagnetic coupling. When the resonant frequency of the resonant loop is close to the resonant frequency of the antenna itself, it can be considered to broaden the impedance bandwidth of the antenna [21], [22]. Moreover, observing Fig. 7(b), the antenna has a partial reverse current after adding the L-shaped parasitic branches, which further illustrates that the L-shaped parasitic structure can be seen as a reflective surface that improves the isolation of the MIMO antenna [23].

The dimensions of the proposed antenna are optimized by the electromagnetic simulation tool CST. Finally, the optimal design parameters of the UWB MIMO antenna are set as follows: $L = 35$ mm, $L_1 = 5.1$ mm, $L_2 = 0.3$ mm, $L_3 = 12.5$ mm, $L_4 = 17.25$ mm, $W = 50$ mm, $W_1 = 1.5$ mm, $W_2 = 7.5$ mm, $W_3 = 1$ mm, $W_4 = 5$ mm, $W_5 = 16.75$ mm, $W_6 = 0.5$ mm, $W_7 = 0.5$ mm, $R_1 = 9.5$ mm, and $R_2 = 15$ mm.

## III. Results Analysis

### A. S-Parameters

Fig. 8(a) presents the prototype of the fabricated antenna. Fig. 8(b) shows that the measured and simulated *S*-parameter curves are basically consistent. The measured frequency range of the UWB MIMO antenna is 3–11 GHz, which satisfies the UWB application. Moreover, the proposed antenna has an isolation of more than 25 dB over the whole operating bandwidth, which is better than that of the antennas reported in [9] and [13]–[15].

### B. Radiation Patterns, Gain, and Efficiency

The two-dimensional (2-D) radiation patterns of the proposed design are simulated and measured at three frequencies, namely, 3.5, 6.5, and 9.5 GHz. In Fig. 9, the proposed design exhibits a good omnidirectional mode on the H-plane, and the pattern of the E-plane is similar to the "8" shape of the conventional monopole antenna. Then, as depicted in the inserted 3-D radiation patterns, as the frequency increases, the radiation pattern of the MIMO

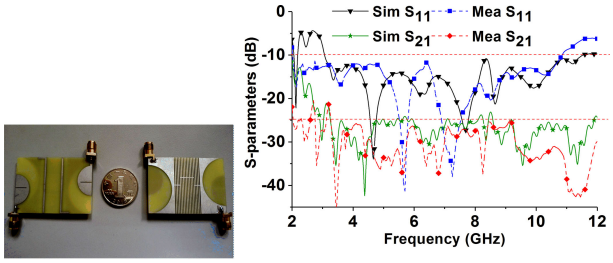


Fig. 8. (a) Photograph of the fabricated antenna. (b) Simulated and measured $S_{11}$ and $S_{21}$ of the proposed design.

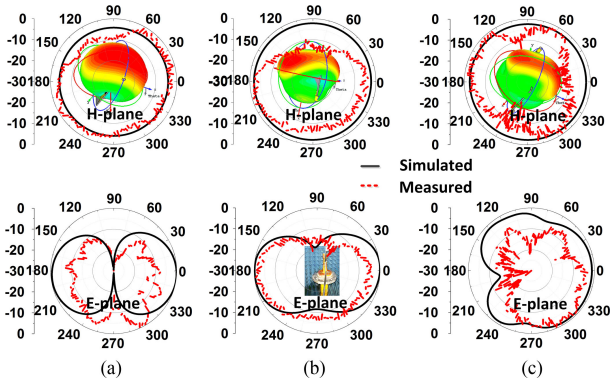


Fig. 9. Radiation patterns: (a) 3.5 GHz, (b) 6.5 GHz, and (c) 9.5 GHz.

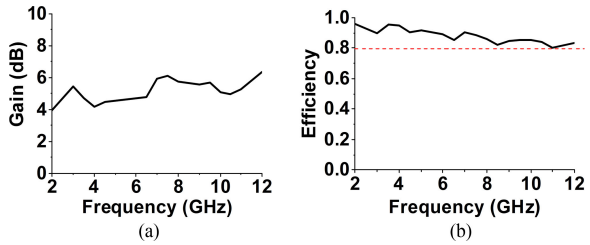


Fig. 10. Simulated results of the proposed antenna. (a) Gain. (b) Efficiency.

antenna changes. The change is caused by the imbalance of the high-frequency current distribution. However, this radiation characteristic facilitates the formation of angular diversity (also known as pattern diversity) for MIMO antennas.

Fig. 10(a) depicts the antenna gain curve as the frequency changes, the results of which indicate that the antenna gain in the operating bandwidth of 3–11 GHz is basically above 3 dB. Fig. 10(b) shows that the antenna has stable radiation efficiency, being above 80% in the operating frequency band.

### C. Diversity Characteristics

For MIMO antennas, the ECC ($\rho_{eij}$) is used to indicate the correlation between the antenna elements. A lower ECC indicates a higher diversity gain. The ECC calculated from the *S*-parameters is approximated for an ideal uniform scattering environment. To obtain calculation results that can reflect the actual situation, the

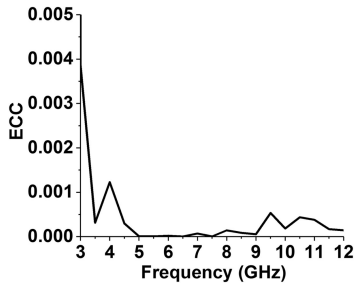


Fig. 11. Simulated ECC of the proposed design.

TABLE I
PERFORMANCE COMPARISONS WITH THE PREVIOUSLY REPORTED LITERATURE

| References | Antenna size ($mm^2$) | Bandwidth (GHz) | Isolation (dB) | ECC |
|---|---|---|---|---|
| [9] | 50 × 28 | 2.8-11.5 | > 18 | < 0.05 |
| [11] | 80 × 48 | 3.1-10.6 | > 25 | --- |
| [13] | 41.5 × 26.75 | 3.1-11.5 | > 19 | < 0.01 |
| [14] | 95 × 60 | 2.5-4.5 | > 18 | < 0.15 |
| [15] | 91 × 38 | 2.8-10 | > 22 | < 0.05 |
| This work | 50 × 35 | 3.0-11 | > 25 | < 0.004 |

ECC is numerically computed using far-field radiation patterns according to (1) [24]. Observing Fig. 11, the ECC is very low (ECC $< 0.004$) in the operating band, which means that the proposed design has outstanding characteristics of lower correlation and higher diversity gain.

In (1) shown at the bottom of this page, *i* and *j* are the numbers of ports, *XPR* is the cross-polarization ratio, and $P_\theta$ and $P_\varphi$ are the $\theta$ and $\varphi$ components of the angular density functions of the incoming wave, respectively. $\Omega$ is the solid angle of the spherical coordinate.

To highlight the novelty of this letter, Table I lists a comparison of the performances of the antenna between this letter and the literature [9], [11], [13]–[15]. Compared with the antennas reported in [14] and [15], the proposed antenna has more compact size and higher isolation. In addition, the proposed antenna has a wider operating bandwidth than that in [14]. Although the isolation in [11] is the same as that in this letter, the size of the antenna in [11] is more than twice the size of that in this letter.

## IV. CONCLUSION

A novel fence-type decoupling structure was presented to enhance the isolation of the MIMO antenna in this letter. Furthermore, two L-shaped parasitic branches were introduced on the surface of the dielectric substrate, aiming at improving the low-frequency (3–3.4 GHz) mutual coupling and impedance-matching performance. The experimental results prove that the proposed design has a high isolation ($S_{21} > 25$ dB) in the operating bandwidth (3–11 GHz), which means that the proposed design is an outstanding choice for portable UWB communication systems. Moreover, a lower ECC (ECC $< 0.004$) illustrates that the antenna has better diversity performance.

$$\rho_{eij} = \frac{\left|\int_0^{2\pi}\int_0^{\pi}\left(\mathrm{XPR}\cdot E_{\theta i}\cdot E_{\theta j}^{*}\cdot P_\theta + E_{\varphi i}\cdot E_{\varphi j}^{*}\cdot P_\varphi\right)d\Omega\right|^2}{\int_0^{2\pi}\int_0^{\pi}\left(\mathrm{XPR}\cdot E_{\theta i}\cdot E_{\theta i}^{*}\cdot P_\theta + E_{\varphi i}\cdot E_{\varphi i}^{*}\cdot P_\varphi\right)d\Omega \times \int_0^{2\pi}\int_0^{\pi}\left(\mathrm{XPR}\cdot E_{\theta j}\cdot E_{\theta j}^{*}\cdot P_\theta + E_{\varphi j}\cdot E_{\varphi j}^{*}\cdot P_\varphi\right)d\Omega}. \quad (1)$$

## REFERENCES


[1] F. Z. T. Kaiser, *Ultra Wideband Systems With MIMO*. Hoboken, NJ, USA: Wiley, 2010.

[2] I. Oppermann, M. Hamalainen, and J. Iinatti, *UWB Theory and Applications*, vol. 1. New York, NY, USA: Wiley, 2004, pp. 3–4.

[3] K. Wei, Z. Zhang, W. Chen, and Z. Feng, "A novel hybrid-fed patch antenna with pattern diversity," *IEEE Antennas Wireless Propag. Lett.*, vol. 9, pp. 562–565, 2010.

[4] T. Kaiser, Z. Feng, and E. Dimitrov, "An overview of ultra-wideband systems with MIMO," *Proc. IEEE*, vol. 97, no. 2, pp. 285–312, Feb. 2009.

[5] C. A. Balanis, *Antenna Theory: Analysis and Design*, 3rd ed. Hoboken, NJ, USA: Wiley, 2005.

[6] J. Banerjee, R. Ghatak, and A. Karmakar, "A compact planar UWB MIMO diversity antenna with Hilbert fractal neutralization line for isolation improvement and dual band notch characteristics," in *Proc. Int. Conf. Emer. Trends Electron. Devices Comput. Techn.*, Kolkata, India, 2018, pp. 1–6.

[7] S. Zhang and G. F. Pedersen, "Mutual coupling reduction for UWB MIMO antennas with a wideband neutralization line," *IEEE Antennas Wireless Propag. Lett.*, vol. 15, pp. 166–169, 2016.

[8] N. Jaglan, S. D. Gupta, E. Thakur, D. Kumar, B. K. Kanaujia, and S. Srivastava, "Triple band notched mushroom and uniplanar EBG structures based UWB MIMO/diversity antenna with enhanced wideband isolation," *Int. J. Electron. Commun.*, vol. 90, pp. 36–44, 2018.

[9] A. A. Ibrahim, J. Machac, and R. M. Shubair, "Compact UWB MIMO antenna with pattern diversity and band rejection characteristics," *Microw. Opt. Technol. Lett.*, vol. 59, no. 6, pp. 1460–1464, 2017.

[10] B. P. Chacko, G. Augustin, and T. A. Denidni, "Uniplanar slot antenna for ultra wideband polarization-diversity applications," *IEEE Antennas Wireless Propag. Lett.*, vol. 12, pp. 88–91, 2013.

[11] N. Gogosh, M. F. Shafique, R. Saleem, I. Usman, and A. M. Faiz, "An UWB diversity antenna array with a novel H-type decoupling structure," *Microw. Opt. Technol. Lett.*, vol. 55, no. 11, pp. 2715–2720, 2013.

[12] Z.-X. Yang, H.-C. Yang, J.-S Hong, and Y. Li, "A miniaturized triple band-notched MIMO antenna for UWB application," *Microw. Opt. Technol. Lett.*, vol. 58, no. 3, pp. 642–647, 2016.

[13] J. Banerjee, A. Karmakar, R. Ghatak, and D. R Poddar, "Compact CPW-fed UWB MIMO antenna with a novel modified Minkowski fractal defected ground structure (DGS) for high isolation and triple band-notch characteristic," *J. Electromagn. Waves Appl.*, vol. 31, no. 15, pp. 1550–1565, 2017.

[14] Y. Wu and Q. Chu, "Dual-band multiple input multiple output antenna with slitted ground," *Microw., Antennas Propag.*, vol. 8, no. 13, pp. 1007–1013, Oct. 21, 2014.

[15] M. Jusoh, M. F. Jamlos, M. R. B. Kamarudin, and M. F. B. A. Malek, "A MIMO antenna design challenges for UWB application," *Prog. Electromagn. Res. B*, vol. 36, pp. 357–371, 2012.

[16] M. Sun, Y. P. Zhang, and Y. Lu, "Miniaturization of planar monopole antenna for ultrawideband radios," *IEEE Trans. Antennas Propag.*, vol. 58, no. 7, pp. 2420–2425, Jul. 2010.

[17] L. Wu, Y. Xia, X. Cao, and Z. Xu, "A miniaturized UWB-MIMO antenna with quadruple band-notched characteristics," *Int. J. Microw. Wireless Technol.*, vol. 10, pp. 948–955, 2018.

[18] A. T. Mobashsher and A. Abbosh, "Utilizing symmetry of planar ultra-wideband antennas for size reduction and enhanced performance," *IEEE Antennas Propag. Mag.*, vol. 57, no. 2, pp. 153–166, Apr. 2015.

[19] J. Liu, K. P. Esselle, S. G. Hay, and S. Zhong, "Effects of printed UWB antenna miniaturization on pulse fidelity and pattern stability," *IEEE Trans. Antennas Propag.*, vol. 62, no. 8, pp. 3903–3910, Aug. 2014.

[20] J. Ren, W. Hu, Y. Yin, and R. Fan, "Compact printed MIMO antenna for UWB applications," *IEEE Antennas Wireless Propag. Lett.*, vol. 13, pp. 1517–1520, 2014.

[21] V. Sharbati, P. Rezaei, and M. M. Fakharian, "A planar UWB antenna with switchable single/double band-rejection Characteristics," *Radioengineering*, vol. 25, no. 3, pp. 429–435, Sep. 2016.

[22] M. Ojaroudi, S. Yazdanifard, N. Ojaroudi, and R. A. Sadeghzadeh, "Band-notched small square-ring antenna with a pair of T-shaped strips protruded inside the square ring for UWB applications," *IEEE Antennas Wireless Propag. Lett.*, vol. 10, pp. 227–230, 2011.

[23] T. K. Roshna, U. Deepak, V. R. Sajitha, K. Vasudevan, and P. Mohanan, "A compact UWB MIMO antenna with reflector to enhance isolation," *IEEE Trans. Antennas Propag.*, vol. 63, no. 4, pp. 1873–1877, Apr. 2015.

[24] M. S. Khan, A. Capobianco, A. I. Najam, I. Shoaib, E. Autizi, and M. F. Shafique, "Compact ultra-wideband diversity antenna with a floating parasitic digitated decoupling structure," *Microw., Antennas Propag.*, vol. 8, no. 10, pp. 747–753, Jul. 15, 2014.